# Essential Elements of the High Density H-Mode on W7-AS

K.McCormick, R.Burhenn, P.Grigull, J.Baldzuhn, S.Bäumel, R.Brakel, H.Ehmler, F.Gadelmeier, L.Giannone, M.Hirsch, E.Holzhauer[1], Y.Igitkhanov, R.Jaenicke, S.Klose, J.P.Knauer, E.Pasch, H.Thomsen, A.Werner, the W7-AS, ECRH and NBI-Teams

*Max-Planck-Institut für Plasmaphysik, EURATOM Ass., 85748 Garching, Germany*
*[1] Institut für Plasmaforschung, Universität Stuttgart, 70569 Stuttgart, Germany*

**Abstract:** The **H**igh **D**ensity **H**-Mode (HDH), discovered during the run-in phase of W7-AS divertor operation /1-3/, rapidly became the workhorse of the divertor program, combining optimal core behavior along with edge parameters necessary for successful operation of an Island Divertor. Its unique properties of high energy confinement along with low impurity retention and radiation localized at the edge under ELM-free steady-state conditions at high densities (to 4 $10^{20}m^{-3}$) and heating powers (to $1.7MWm^{-3}$) make the HDH H-mode ideal for a reactor scenario, given it can be extended to higher temperatures in a larger machine. Hence, considerable effort has been invested to understand the nature of the HDH-mode in order to be able to extrapolate to next generation devices. To this end the present paper reports on experiments where two globally-similar ELM-free H-modes are compared: the classic quiescent H-mode H* where both impurity and density control are a severe problem and the HDH-mode with its contrasting steady-state behavior. Through modeling of the temporal behavior of laser-ablated aluminum spectral lines, as well as that of background impurities, it is concluded that a principle difference between the two H-modes is that of enhanced impurity diffusion in the edge gradient region of the HDH-mode. However, no direct indicators of enhanced diffusion have yet been identified.

## 1. Introduction:

Early 3D modeling calculations for the W7-AS 5/9 island divertor configuration predicted that very high separatrix densities $n_{es}$, approaching $10^{20}$ $m^{-3}$, were going to be necessary to effect plasma detachment at the target plates /4/. Thus, even at the very beginning of divertor studies, emphasis was laid upon attaining high core and associated high edge densities. Experience from past operation with inboard sector limiters dictated that such a regime could be realized only transiently in a steep $n_e$-ramp, since a loss of density control as well as an intolerably high level of radiation $P_{rad}$ was inherently associated with higher densities /5, 6/. However, in contrast to established experience, it was discovered that by utilizing fast $n_e$-ramps a high energy-confinement regime could be accessed which exhibited good density control and no impurity accumulation /1/. Detailed investigations revealed that a $P_{nbi}$-dependent density threshold $n_e^{th}$ existed beyond which this regime – the High Density H-Mode - could be maintained in steady-state /2/. Section 2 deals with plasma phenomenology associated with operation in the vicinity of $n_e^{th}$. In particular, mechanisms by which the H-

mode is achieved under these conditions on W7-AS are discussed, in addition to the general nature of the NC-HDH transition.

Below $n_e^{th}$ the normal-confinement regime (NC) exists, which as the antitheses to the HDH-mode is characterized by poor energy confinement $\tau_E$, laser-ablated Al-confinement times $\tau_{Al}$ more than 30 times $\tau_E$ and central peaking of $P_{rad}$. Early investigations revealed that the differences in energy confinement between the NC- and HDH-modes were related to the much broader density profiles of HDH, in contrast to the peaked profiles of NC /2/. Further, the diminished residence time of laser-ablated aluminum (LBO) in HDH compared to NC could be modeled in an ad hoc fashion by a smaller inwards impurity pinch in the core plasma /2, 7 /. In fact, the peaked $n_e$-profiles of NC are neoclassically predicted to provoke impurity accumulation. In addition, neoclassical calculations indicated that temperature screening together with the flat $n_e$-profiles could be the physical factors for the lack of central impurity accumulation in HDH /8/. However, the inward convection associated with steep density gradients at the plasma edge for HDH would nonetheless still contrive to effectively confine impurities within the core plasma. A postulation of enhanced impurity diffusion at the plasma edge was necessary in order to reproduce the impurity flushing features of HDH /8, 9, 10/.

The classical quiescent H-mode H* has $n_e$ - and $T_e$ -profiles similar to HDH, but in stark contrast to HDH exhibits strong impurity accumulation, often running into a radiation collapse within a few energy confinement times. In order to provide a back-to-back comparison between H* and HDH, a discharge was tailored which contained both types of H-mode under conditions as identical as possible – with the goal of pinpointing essential operative elements of HDH physics. Section 3 reports on these dedicated studies.

## 2. Formation of the HDH-Regime:

For the standard 5/9 island divertor configuration which formed the basis of initial divertor studies on W7-AS a fast $n_e$-ramp to the target density, via a strong gas puff, was found necessary to reliably attain HDH. Figure 1 gives details of three discharges with flattop densities in the immediate vicinity of $n_e^{th}$. All have essentially the same initial gas puff rate (not shown) and density buildup, but the slight differences in final density lead to dramatically different global behavior.

All discharges start with nearly the same stored energy W, which suggests similar $n_e$ - and $T_e$-profile shapes in this phase. However, the lowest density discharge (red traces) suffers a transition to lower W within 100ms. This is accompanied by ELM-like activity, seen in the $H_\alpha$ trace. The next highest density, only a few percent more, preserves its maximum W for several 100ms before lapsing to the same lower W. Again, the high-confinement phase is apparently ELM-free. Finally, the 3$^{rd}$ discharge maintains W until cessation of $P_{nbi}$ (around 1sec). Further, there is no evident ELM activity throughout. Among these discharges the behavior of $P_{rad}$ is notable: For the lowest density $P_{rad}$ increases throughout the discharge. For

the middle value $P_{rad}$ attains constancy in the high-W phase about 100ms after the highest-$n_e$ discharge has come into equilibrium. Thus, the confinement time of impurities is also a strong function of density in this range. This is validated by dedicated LBO studies of Al, where $\tau_{Al}$ strongly drops directly after crossing the NC-HDH threshold /2/.

The global energy confinement time $\tau_E$ for a series of discharges at different $n_e$ is depicted in Figure 2. The blue points are derived from "steady-state" phases of each discharge, i.e. in the case of the NC-regime after W has relaxed to its lowest value. In contrast, the red points are taken from the maximum transient value of W attained for NC-discharges – at the beginning where profile formation is still affected by the density buildup. Two aspects emerge from this form of $\tau_E$ vs $n_e$ plot: a) The transition from NC to HDH conditions is not absolutely sharp in terms of a threshold density. Rather the transition density signifies attainment of a self-sustaining condition. b) Considering the transiently high $\tau_E$ values of NC discharges, the increase of $\tau_E$ vs. $n_e$ up to values around 2.2 $10^{20}m^{-3}$ (for 2MW neutral injection) is continuous and much faster than the scaling predicted by the ISS95 scaling of $\tau_E \sim n_e^{0.5}$ /11/.

Figure 3 gives the NC-HDH existence diagram for three heating levels, $P_{nbi}^{abs} \sim 0.7$, 1.4 and 2.4MW. There is an evident increase in $n_e^{th}$ with power. The scaling is roughly $n_e^{th} \sim 1.67\ P_{nbi}^{abs\ 0.28}[10^{20}\ m^{-3}, MW]$. Note that the HDH phase is maintained to the vicinity of the W7-AS density limit for limiters /12/. The density limit for the divertor situation is always exceeded since in this case it is defined as being that density where W begins to roll over /13/.

Present thinking with respect to the formation of HDH conditions considers the influence of NBI particle deposition, which is more central, and edge fueling by gas puffing, which at high densities is concentrated at the very periphery. The supposition is that if radial particle diffusion is slower than the buildup rate of density at the edge – also taking into account the NBI deposition - then the gas puff is able to drive a steep edge density gradient /2, 14-15/. Experimentally, this effect has already been observed in fast density ramps in a poloidal limiter situation on W7-AS /5, 6/. The result of steeper gradients is to produce a stronger radial electrical field which enhances poloidal plasma spinup and sheared flow, eventually leading to suppression of turbulence and H-mode conditions. Such a scenario has been simulated in model calculations /14-15/. Since this process also involves overcoming the more central deposition of NBI, high $P_{nbi}$ will automatically require a higher gas puff rate and thus a higher density before a balance is attained and a steady-state situation is possible. Note that in contrast to the circumstance of a tokamak, this balance becomes easier to achieve at higher $n_e$, since perpendicular diffusion is found to decrease with $n_e$ on W7-AS /16/. Another potentially relevant factor for the $n_e^{th}$ power scaling is the observation that the H-mode power threshold on W7-AS behaves in a contrary fashion to tokamaks: On W7-AS an increase in $P_{nbi}$ leads to poorer H-mode confinement, or even loss of the H-mode, which can be regained by increasing the density /5, 17/.

These propositions are advanced to explain the formation of flat H-mode $n_e$-profiles from the peaked profiles associated with NC (examples in fig. 4). They are not able to provide a solution to the impurity behavior of HDH. To this end a simple ad-hoc model furnishes a possible explanation: Assuming that inward impurity convection is proportional to the local pressure gradient, it is also necessary to invoke an enhanced diffusion coefficient in the gradient region in order to counteract the predicted high inwards convection there (Fig. 4). Otherwise, impurities are confined within the transport barrier. However, with these combined assumptions, it is possible to nicely reproduce the temporal decay of emission lines from Al injected via LBO into the core plasma /8-10/.

The next section deals with an experiment directly designed to study intimate differences between H*- and HDH-phases of one discharge, with the intent of revealing the "HDH-activator" or at least differences associated with the radically variant modes of impurity confinement.

## 3. Study of H*- and HDH-Modes:

A discharge was tailored in an island-divertor configuration with $P_{nbi}^{abs}$ ~1.4MW whereby the density was ramped up until attainment of H*, and then after a 60ms plateau increased again until the HDH mode was solidly established (Fig.5). Hereby a magnetic configuration was chosen where $\iota_a$ (0.561) was better placed in the classical H-mode window in $\iota_a$-space /5, 18/, since the standard divertor configuration ($\iota_a$~0.567) did not permit attainment of H* at these power levels. Further, a smaller island size was adjusted via the control coils /1/ in order to more readily permit undisturbed density feedback regulation via the HCN interferometer. Thus, the effective plasma radius was ~ 14.2cm (vs. 12cm) and the x-point to target plate distance was ~ 0.8cm (vs. 3.8cm). The discharge depicted in Fig. 5 was repeated often, allowing dedicated shots for many different diagnostics.

The entrance into H* is indicated by the cessation of prominent ELM activity (seen in $H_\alpha$ of Figs. 5 & 6), followed by a rapid increase in global radiation $P_{rad}$ as registered by a bolometer array. A constant density plateau during H* was enabled by He glow-discharge cleaning before each series discharge in order to promote pumping by the graphite divertor target plates. (Not necessary for pure HDH discharges.) Otherwise, $n_e$ normally rises during H* at such high densities. The maximum length of the H* plateau was dictated by the goal of a good transition to HDH within the same discharge. While setting up the scenario it was seen that a delay of the 2$^{nd}$ $n_e$-ramp by only another 10ms lead to unavoidable radiation collapse. For the scenario developed here, the $n_e$-ramp stops the runaway of impurity radiation ($P_{rad}$ of Fig. 5 & FeXVI of Fig. 6). Simultaneously, the radiation moves outwards, shown by the temporal evolution of bolometer chords at ~2/3 radius and the plasma edge (10 & 16cm traces of Fig. 6). The $P_{rad}$ profiles (Fig.8, top) illustrate that the initially flat distribution at the start of H* (0.315s) quickly changes to a hollow profile whose amplitude increases with time. In

contrast, the transition to HDH is accompanied by a dramatic peaking of $P_{rad}(r)$ outside the confinement region, with little change in the global radiation level.

The density increase needed to provoke the H*->HDH transition leads to a marginal augmentation of plasma energy (i.e. similar pressure profiles), but the decay times for laser-ablated aluminum are radically different: no falloff of AlXII radiation is observed over the H*-phase, whereas for HDH the e-folding time constant is the order of 100ms /10/. The $n_e$- and $T_e$-profiles for H* and HDH (Fig. 7) are evidently of the same form, so a change in impurity transport based largely on $n_e$-profile shapes – as for NC and HDH – cannot find application. Perhaps of significance is that the collisionality $\nu^*$ ($\nu_{ii}R/v_t\iota_a$) for HDH is more than a factor of two higher (Fig. 7, bottom). Nonetheless, in both cases $C^{6+}$ is collisional and $H^+$ is marginally collisionless over most of the radius: These are necessary conditions for neoclassical temperature screening to play a role, leading largely to an outwards-directed impurity flux in the core plasma.

As an anecdote it is remarked that the $n_e$ -profiles of Fig. 7 do not exhibit the same steep gradient at the edge as the profiles of Fig. 4. This is an artifact of the Thomson data associated with the system used to generate the profiles for Fig. 7, which has not been rectified as of this writing. Supplementary information gives no indication that the edge transport barrier gradients are actually any less steep. Here the profiles are shown only to demonstrate there are no pronounced differences in form between H* and HDH and to establish the general level of collisionality.

The temporal behavior of ablated aluminum as well as the qualitative form of the $P_{rad}(r)$ profiles can be described by assuming no difference in transport between H* and HDH in the core plasma, and enhanced impurity diffusion for HDH in the steep gradient region. The effect is to drive impurities to the vicinity of the H-mode edge transport barrier in both cases. For H*, without enhanced diffusion in the gradient region, impurities then accumulate with a hollow radiation profile, whereas for HDH they are flushed further to the outside. Fig. 8 illustrates the behavior of $P_{rad}(r)$ for such model conditions, juxtaposed against $P_{rad}(r)$ from experiment. Qualitatively, all observed $P_{rad}$ features are reproduced: a hollow profile in H* with peaking near the transport barrier and increasing with time, and a stationary $P_{rad}$ profile peaked strongly to the outside for HDH.

Within these considerations no definitive statements are possible concerning background ion transport. The fact that the radial $E_r$-field (Figs. 5-6), as measured by a passive BIV system viewing along an edge chord, is higher in H* may indicate steeper pressure profiles. The uncertainly arises due to imprecise knowledge of the radial origin of the BIV radiation shell as a function of density, i.e. a density increase could in principle effect a radial shift of the shell. On the other hand, the fact that $T_e^{ped}$ at the top of the density pedestal roughly tracks the passive $T_i$ measurement speaks against a large shift. Also speaking for a progressively steeper pressure gradient in H* is the temporal coincidence of the separatrix density $n_{es}$

(decreasing with time for constant $n_e$ implying steeper profiles, if the pedestal density remains constant) and $E_r(t)$ (increasing with time -> steeper profiles). Unfortunately, the dedicated edge Thomson scattering system, which has the necessary spatial resolution to address small changes in profile forms, produced data which one has not yet been able to readily interpret.

## 4. Discussion and Summary:

It has been established in early HDH work that a hard gas puff was necessary to gain access to the HDH regime. Of course, even under normal circumstances a rapid $n_e$ increase is of use in transiently establishing a high density before impurity accumulation and high central radiation becomes a problem. However, here it is postulated that essentially this forces the formation of an H-mode-like $n_e$ edge profile, which leads to buildup of a radial electric field, sheared poloidal flow and suppression of turbulence. Finally, above a certain threshold density $n_e^{th}$ the situation must become self-sustaining without the driving mechanism of a strong exterior gas puff. Simultaneously, upon attainment of the HDH state, an enhanced transport mechanism in the edge barrier region materializes which serves to flush impurities from the core and perhaps is also responsible for the reaching of a steady-state density. Here it is important to realize that the NBI electron fueling rate for 2MW NBI is ~2 $10^{20}$ $s^{-1}$, i.e. in steady-state at least this amount is being passively pumped by the carbon target plates.

A consequence of the conjectured importance of competition between more central NBI particle fueling as compared to gas puff edge fueling is that a decrease in NBI power or use of ECRH should permit access to HDH at lower densities, all else being equal. In fact, HDH conditions could not be found for $P_{nbi}$~0.5MW or any level of ECRH power. In the case of $P_{nbi}$, radiation became too dominant with increasing $n_e$ before a transition could be realized. For ECRH it may well be that the cutoff density of 1.2 $10^{-20}$ $m^{-3}$ is simply too low, i.e. the enhancement in energy confinement with higher $n_e$ (see Fig. 2) is an essential factor in the consummation of the HDH state.

An interesting aspect is that the ability to realize H* as well as the required gas puff rate to attain HDH is perhaps a function of configuration. H* could be achieved for the setup of Fig. 5-6, but not for the standard divertor configuration. Further, within a rather moderate density ramp over more than 200ms (not shown) HDH was accessible in the situation of Fig 5-6. This may reflect operation in that part of the H-mode $\iota_a$-window where neoclassical viscous damping of poloidal ExB rotation is lower than for the standard divertor configuration /19-20/. However, even though viscous damping is generally expected to be smaller in the Pfirsch-Schlüter regime (in particular for the low $T_e$ of the HDH regime) even a marginal influence might be importance in cases of operation near a threshold. In any case, the effect would be to place reduced requirements on the $E_r$ necessary to achieve the required poloidal spinup and thus also reduced demands on the edge density gradient – which would translate into a lower puff rate to achieve the same result. Such an effect would bode well for operation

on W7-X where poloidal viscous damping is minimized /19/. Unfortunately, time did not permit systematic investigations along these lines.

It is of note that the Enhanced $D_\alpha$ H-mode (EDA) of the C-Mod tokamak has properties similar to HDH, e.g. flat $n_e$-profiles with steep edge gradients and steady-state, ELM-free operation without impurity accumulation. A quasi-coherent (QC) mode at the plasma edge is thought to provoke impurity flushing /21-23/. In contrast, ELM-free H-modes without QC exhibit accumulation, just as H* on W7-AS. Finally, impurity transport behavior as well as the pedestal width is consistent with a strong inwards neoclassical impurity pinch in the density gradient region, which to some extent is counteracted by a larger diffusion coefficient for the EDA H-mode in comparison to normal ELM-free H-modes /24/. This strong resemblance to H*-HDH behavior motivated careful examination for similar transport phenomena signatures on W7-AS.

Since an unidentified mechanism is postulated to expel impurities from the edge region in HDH and not in H*, the discharge scenario under discussion in Figs. 5-6 should enable one to more easily discriminate against phenomena not of principle importance for HDH. Mirnov coils mounted on the wall as well as on a fast-scannable probe have been used to register the electromagnetic spectrum in all discharge phases. In contrast to C-Mod where the QC mode is detectable by Mirnov coils only very near the plasma surface (due to the high poloidal number /21/), on W7-AS there is: a) no difference in spectrum between wall-mounted coils and those very near the plasma, b) no strikingly obvious difference in H* and HDH phases, and c) no consistent presence of any particular mode for a variety of HDH discharges – even though it is not uncommon to see weak coherent oscillations in the 80-100kHz range during attached HDH phases and very sharp lines in detachment. The plasma edge has also been probed for density fluctuations using a microwave reflectometer. A dedicated k-scan over $k_\theta \sim$ 0-10$cm^{-1}$ for a frequency range 5-250kHz did not detect any mode activity. The cutoff density of ~6 $10^{19}$ $m^{-3}$ placed the reflecting layer in the density gradient region just inside the separatrix. Measurements at other frequencies, corresponding to cutoff densities of ~8 and 12 $10^{19}$ $m^{-3}$ yielded similar results. An $H_\alpha$ channel viewing the midplane plasma found low-level, low-frequency spectra (<10kHz) in HDH and not H*, whereas the global $H_\alpha$ signal from the divertor module saw no differences. A target plate Langmuir probe sampling an island divertor flux tube from the outer circumference saw spectra similar to the midplane $H_\alpha$ channel while other probes sensitive to inner flux tubes revealed no differences between H* and HDH. These results may point to a poloidal localization of mode activity/turbulence during HDH. Actually, poloidal transport variations in the EDA H-mode on C-Mod were also detected /25/, presumably related to the ballooning character of the QC mode. All in all, the picture concerning HDH-related fluctuations of any nature is not conclusive. More detailed evaluation of experimental material is required. It is already reasonably evident, however, that a Quasi-Coherent mode in the form as present on C-Mod does not exist – which is not

unreasonable since the magnetic field structure at the edge is decidedly different for the two devices.

In any case, high collisionality accompanies HDH closely: HDH has never been found for low-collisionality plasmas. Moreover, since the transition threshold density increases with heating power, it is also difficult to substantially decrease $\nu^*$ by augmenting power. But collisionality is perhaps only one element – as exemplified by the H*-HDH comparison where impurities are in the Pfirsch-Schlüter regime for both cases. Possibly the neutral pressure plays a direct role: The sub-divertor neutral pressure increases more than a factor two during the transition from H* to HDH (Fig. 5) as does the main chamber pressure (not shown, but attaining ~ $10^{-4}$ mbar). Interestingly, an important aspect for an EDA-like mode on the JFT-2M tokamak is thought to be saturated wall conditions leading to high wall recycling and high neutral pressures – thus motivating the name "High Recycling Steady H-Mode" /26/. Another HDH primal factor might be related to the decreasing neutral penetration depth with increasing density. In fact, for HDH regimes the expected penetration depth of 1$^{st}$ generation neutrals is rather close to the density pedestal width. (Keeping in mind that the principle source of neutrals is through recycling at the divertor modules - where magnetic flux expansion exists, leading to a broader local pedestal as compared to that seen in plots of $n_e$ and $T_e$ vs. the effective radius of Fig. 4.)

Of importance is also that the HDH mode can exist in a wide variety of magnetic configurations, including limiter plasmas if the heating power is sufficiently high. Indeed, all high-$\beta$ studies are carried out with configurations having intimate contact with the target plates, and these discharges display essentially HDH characteristics /27/. Thus, a divertor configuration seems not an absolute prerequisite, although it enables far easier and very robust access to HDH and allows penetration to very high densities where divertor detachment is well developed /1, 28-29/. In contrast, evidence is strong that the EDA H-mode is predicated on a resistive ballooning x-point mode /23/ - which would surely take on different characteristics for the 8-10 x-points of W7-AS. Moreover, it should presumably not even be a factor for a limiter plasma (where an x-point is behind the target plate).

Summarizing, the HDH mode may be one of a generic family of "high collisionality" ELM-free H-modes with some form of enhanced (impurity) transport at the edge. As such, it is an outstanding member since it enables steady-state, high-density, high-confinement, high-power operation over the breadth of relevant attached/detached divertor scenarios. Notwithstanding that W7-AS is now decommissioned, hope remains that the extensive HDH-database may yet serve to illuminate the physics base for the HDH H-mode, permitting extrapolation of performance to other machines.

**References**

/1/ P.Grigull et al., Plasma Phys. Control. Fusion 43 (2001) A175
/2/ K.McCormick et al., Phys. Rev. Lett. 89 (2002) 015001

/3/ K.McCormick et al., J. Nucl. Mater. 313-316 (2003) 1131
/4/ Y.Feng et al., 28th EPS Conf. ECA 25A (Madeira, 2001) 1949
/5/ K.McCormick et al., Plasma Phys. Control. Fusion 41 (1999) B285
/6/ K.McCormick et al., J. Nucl. Mater. 290-293 (2001) 920
/7/ R.Burhenn et al., 29th EPS Conf., ECA 26B (Montreux, 2002) P.4.043
/8/ R.Burhenn et al., 30th EPS Conf., ECA 27A (St. Petersburg, 2003) P-1.2
/9/ K.Ida et al., Plasma Phys. Control. Fusion 45 (2003) 1931
/10/ R.Burhenn et al., this conference
/11/ U.Stroth et al., Nuclear Fusion 36 (1996) 1063
/12/ L.Giannone et al., Plasma Phys. Contr. Fusion 44 (2002) 2149
/13/ L.Giannone et al., Plasma Phys. Contr. Fusion 45 (2002) 1713
/14/ Y.Igitkhanov et al., 9th EU-US Transport Task Force Workshop (Cordoba, 2002) O.III.08
/15/ Y.Igitkhanov et al., this conference
/16/ P.Grigull et al., 20th EPS Conf., ECA 17c (Lisbon, 1993) II-739
/17/ P.Grigull et al., J. Nucl. Mater. 290-293 (2001) 1009
/18/ F.Wagner et al., IAEA (Lyon, 2002) OV2-4
/19/ H.Wobig et al., Plasma Phys. Control. Fusion 37 (1995) 893
/20/ H.Wobig et al., Plasma Phys. Control. Fusion 42 (2000) 823
/21/ J.A.Snipes et al., Plasma Phys. Control. Fusion 44 (2001) L23
/22/ D.A.Mossessian et al., Plasma Phys. Control. Fusion 44 (2002) 423
/23/ A.Mazurenko et al., Phys. Rev. Lett. 89 (2002) 22500
/24/ T.Sunn Pedersen et al., Nuclear Fusion 40 (2000) 1795
/25/ T.Sunn Pedersen et al., Physics of Plasmas 9 (2002) 4188
/26/ K.Kamiya et al., Proc. 19th IAEA Conf., IAEA-CN-94-EX/P2-04 (Lyon, 2002)
/27/ A.Weller et al., to be published in Plasma Phys. Control. Fusion
/28/ P.Grigull et al., this conference
/29/ Y.Feng et al., this conference

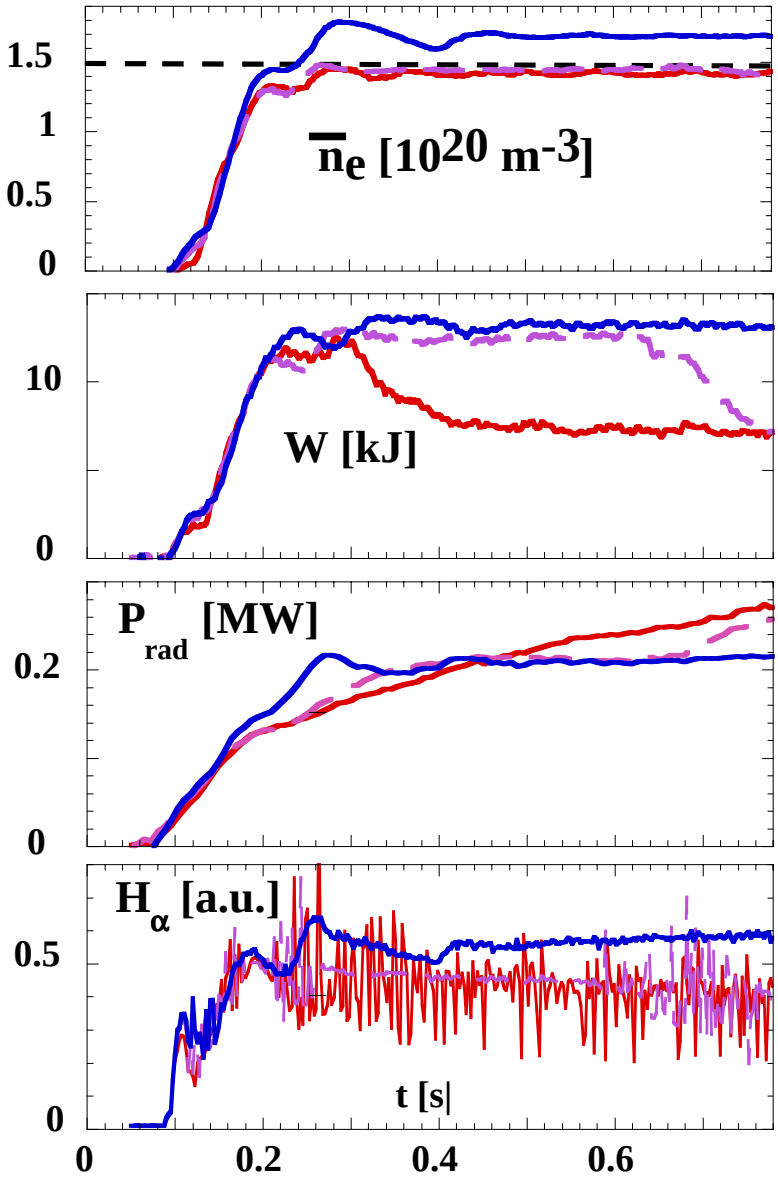


Fig. 1: Temporal behavior of: line-averaged density $n_e$, stored energy W, global total radiated power $P_{rad}$, and $H_\alpha$ from the divertor module region for three discharges with densities near the NC->HDH transition (~1.5 $10^{20}$ $m^{-3}$ at this power level). $\iota_a$=0.567, $a_{eff}$~12cm, x-point distance to target plate ~3.8cm; $B_t$ =-2.5T; $P_{nbi}^{abs}$ ~0.7MW, electron fueling rate from NBI is ~ 1 $10^{20}$ $s^{-1}$. #55595, 96 & 98.

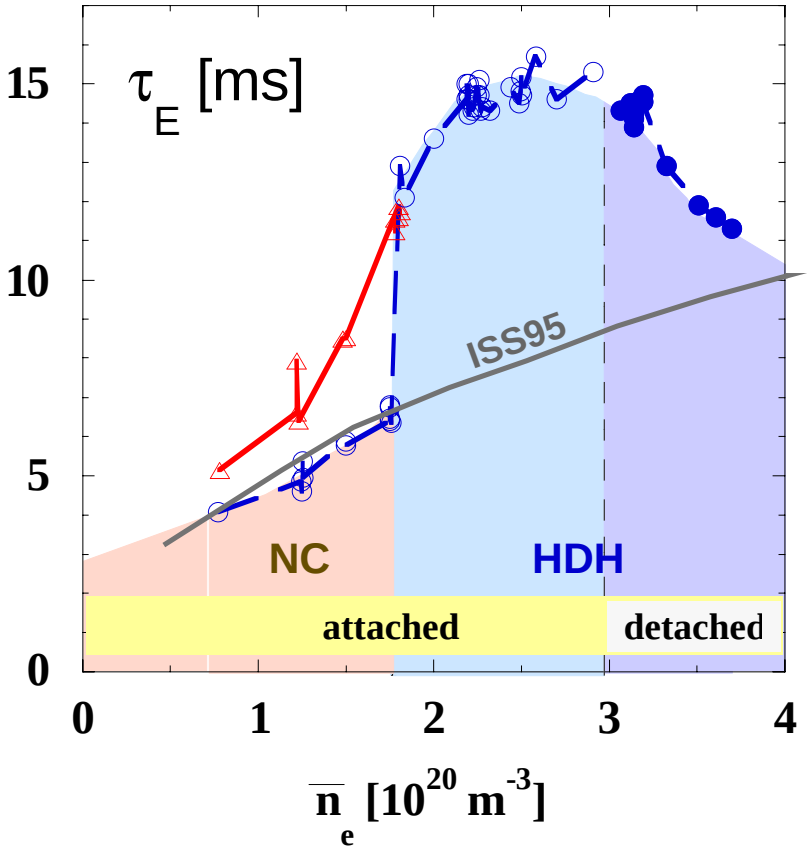


Fig. 2: Energy confinement time $\tau_E$ vs. line-averaged density for the standard island divertor configuration. $\iota_a$=0.567, $a_{eff}$~12cm, x-point distance to target plate ~3.8cm; $B_t$ =-2.5T; $P_{nbi}^{abs}$ ~1.4MW. The blue points are taken from steady-state phases of individual discharges. The red points arise from the transient high-confinement phase of the corresponding discharges in blue. The transition density (~1.8 $10^{20}m^{-3}$) for NC->HDH is indicated, as well as the regions of attached/detached plasmas at the target plate. The International Stellarator Scaling ISS95 /11/ is given as a gray solid line.

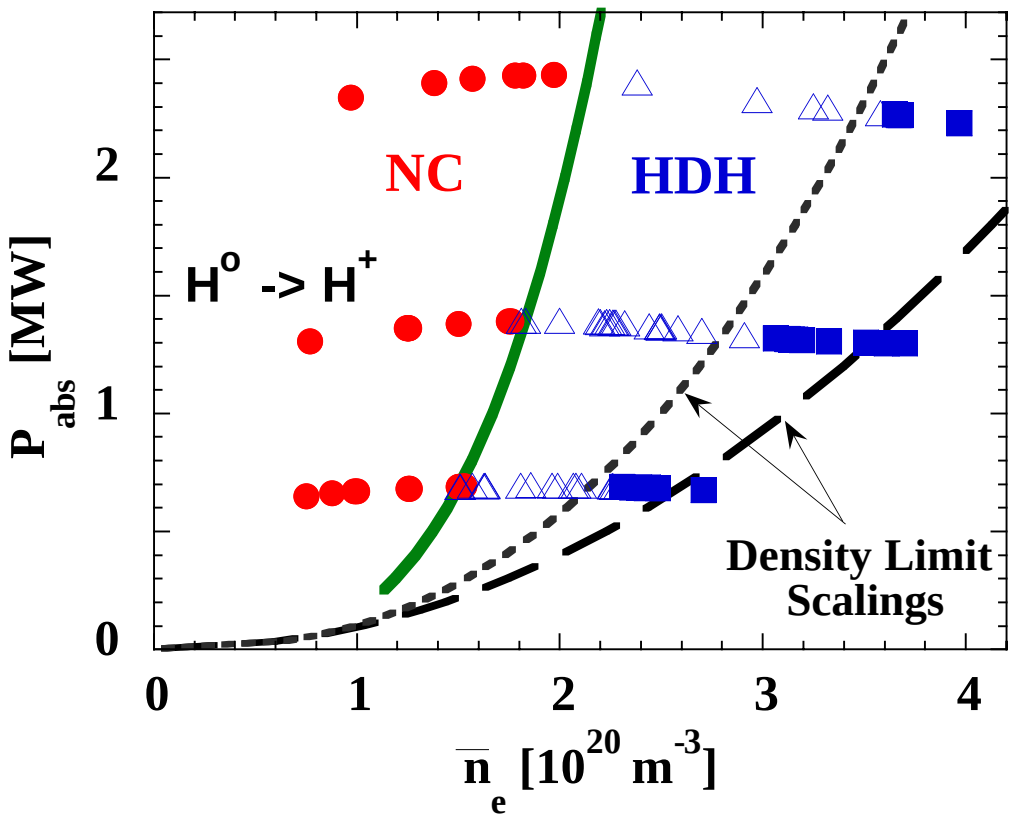


Fig. 3: Existence Diagram for NC (red) and HDH (blue) operational regimes for the standard divertor configuration at three NBI power levels. The NC->HDH transition boundary (green) is indicated (~1.67 $P_{nbi}^{abs\ 0.28}$) as well as two W7-AS density limit scalings: limiter (long dashes) 1.46 $(P^{abs}/V)^{0.48}$ $B_t^{0.54}$ /12/ and divertor (short dashes) 1.5$(P^{abs}/V)^{0.4}$ $B_t^{0.32}$ /13/. Solid blue points correspond to detached discharges.

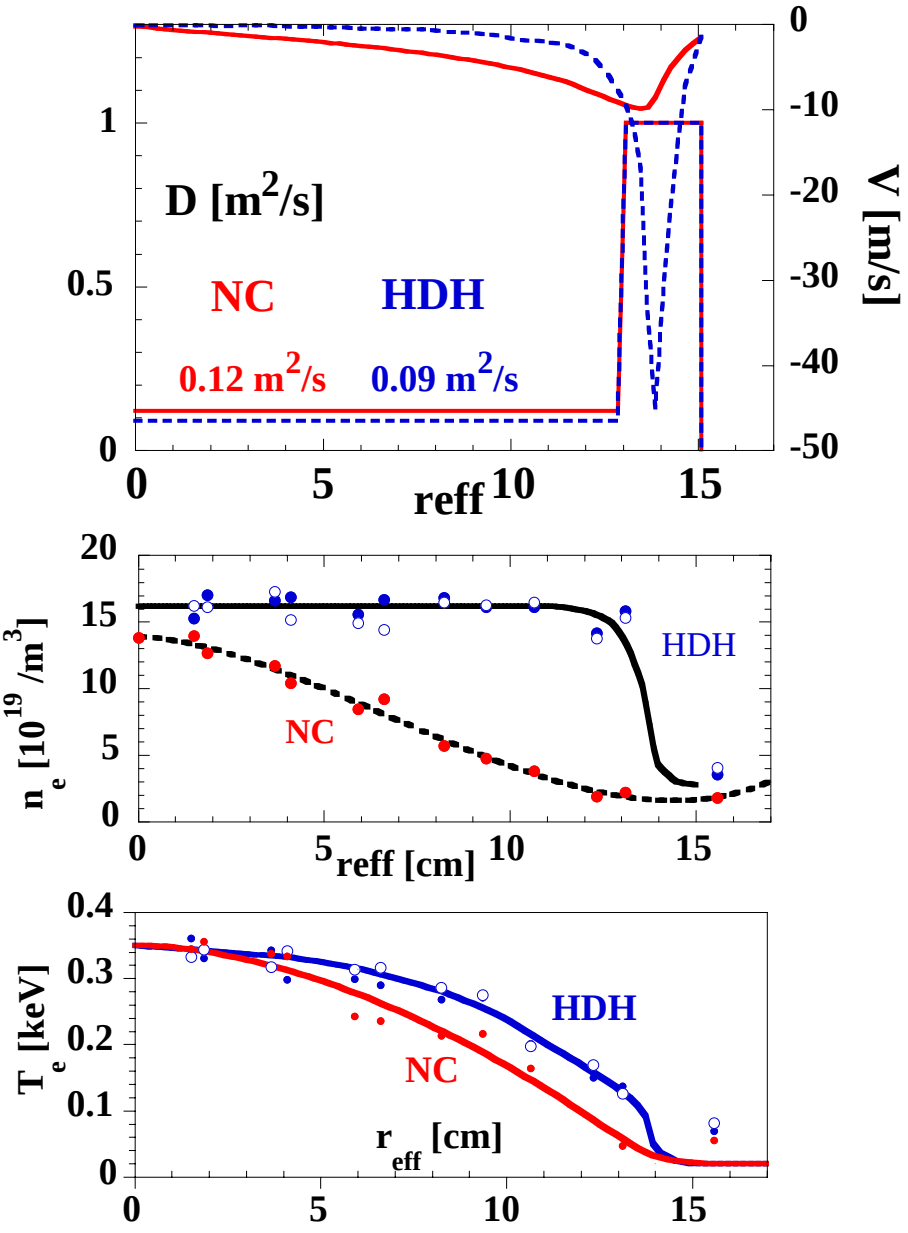


Fig. 4: Bottom: $n_e$- and $T_e$-profiles for two discharges, one displaying normal confinement (#55587) and the other HDH-mode confinement (#55542). Top: Ad hoc transport model for laser-ablated aluminum, with an inward pinch taken proportional to the local pressure gradient. The diffusion constant is held constant at a low value in the core and increased a factor of ten in the gradient region in order to duplicate the HDH waveform for impurity line decay /8/. $B_t$ = -2.5T, $P_{nbi}^{abs}$~0.7MW.

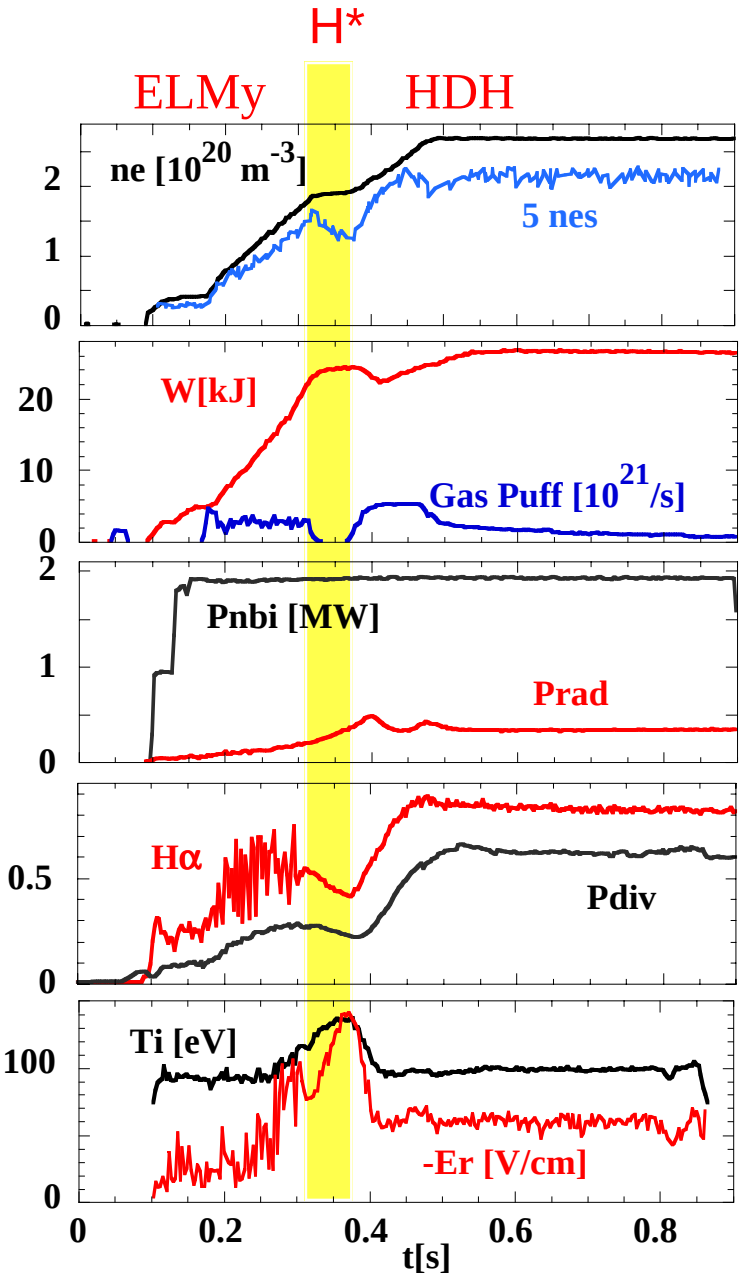


Fig. 5: Line-averaged density $n_e$, density at separatrix $n_{es}$, stored energy W, $H_\alpha$ from divertor region, and subdivertor neutral pressure $P_{div}$. Ion temperature $T_i$ and radial electric field $E_r$ derived from passive observation of a BIV line along a chord in the density gradient region. ELMy, H* and HDH phases are indicated. $\iota_a$ = 0.561, $a_{eff}$~14.2cm, x-point distance to target plate ~0.8cm; $B_t$ = -2.5T; $P_{nbi}^{abs}$ ~1.4MW, electron fueling rate from NBI is ~ 2 $10^{20}$ $s^{-1}$.

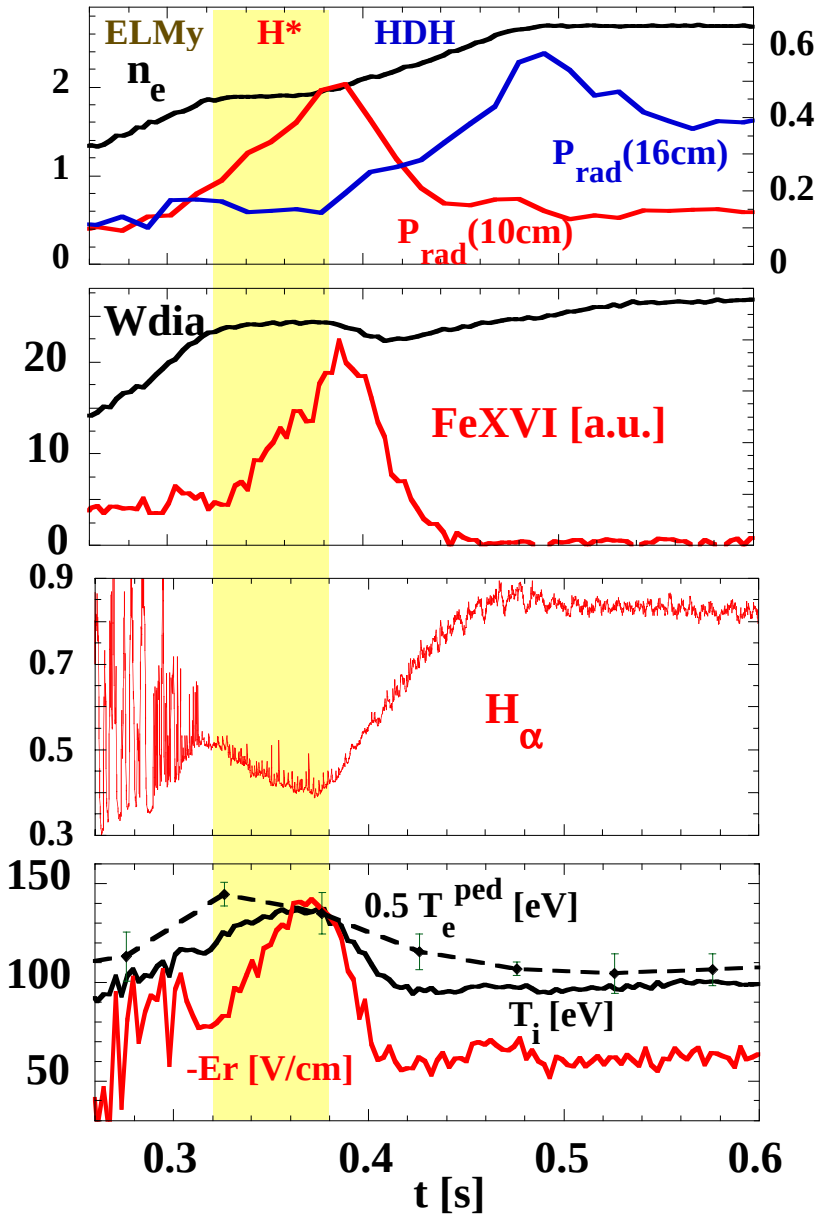


Fig. 6: Expanded time scale from Fig. 5 showing radiation along two bolometer chords $P_{rad}$, at 10 and 16cm from the plasma center, FeXVI line intensity along a center chord and $H_\alpha$ from the divertor. The bottom plot shows the radial electric field $E_r$ and $T_i$, measured along an edge chord by a passive BIV system, and $T_e^{ped}$ at the top of the pedestal (Thomson scattering). The H* phase is indicated.

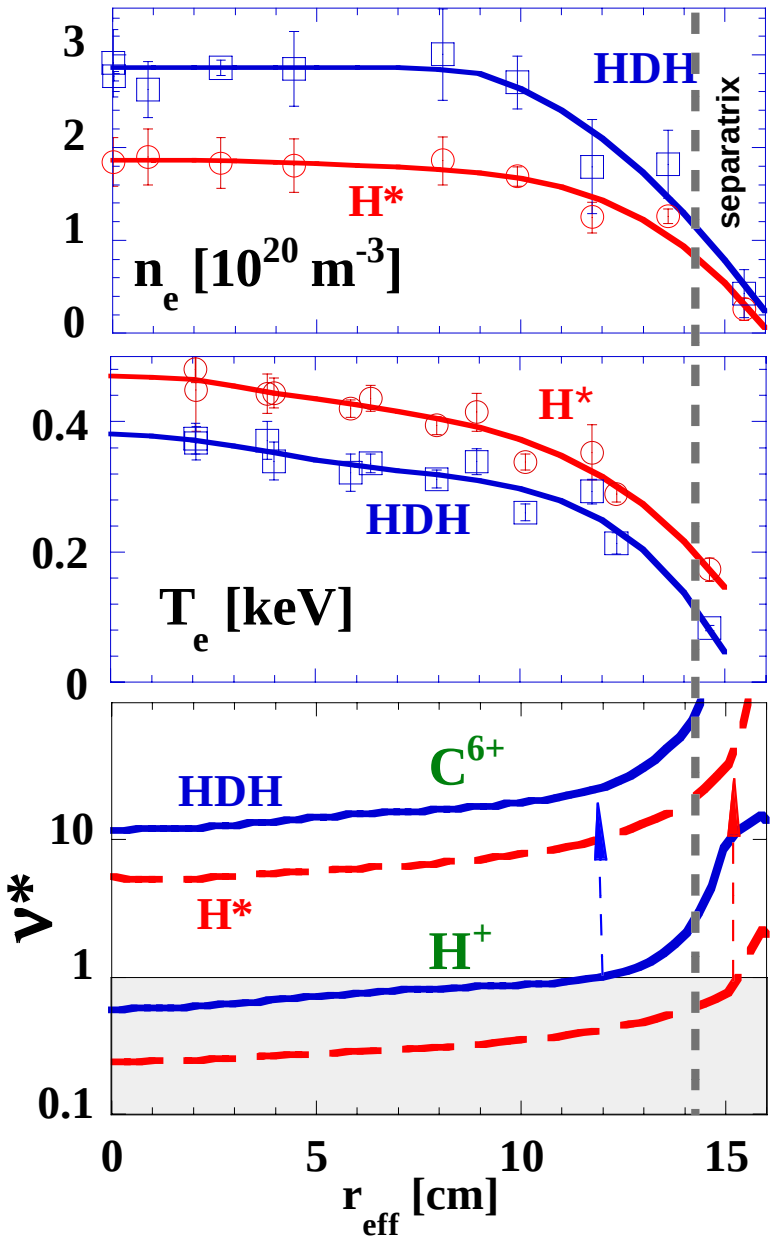


Fig. 7: $n_e$- & $T_e$-profiles for shot of Figs. 5-6. ν* profiles for $C^{6+}$ and $H^+$. ν*= 1 at the junction between the plateau and Pfirsch-Schlüter regimes, i.e. $\nu^* = \nu_{ii}R/v_t\iota_a$, where $\nu_{ii}$ = ion-ion collision frequency, $\iota_a$ = edge iota, $v_t$ = thermal velocity, R = major radius. We see that the collisionality of HDH is more than a factor of two higher. Nonetheless, both regimes are collisional for $C^{6+}$ and marginally non-collisional for $H^+$. The errors mark the radius beyond which $\nu^*(H^+)>1$, i.e. for which temperature screening should no longer be a factor.

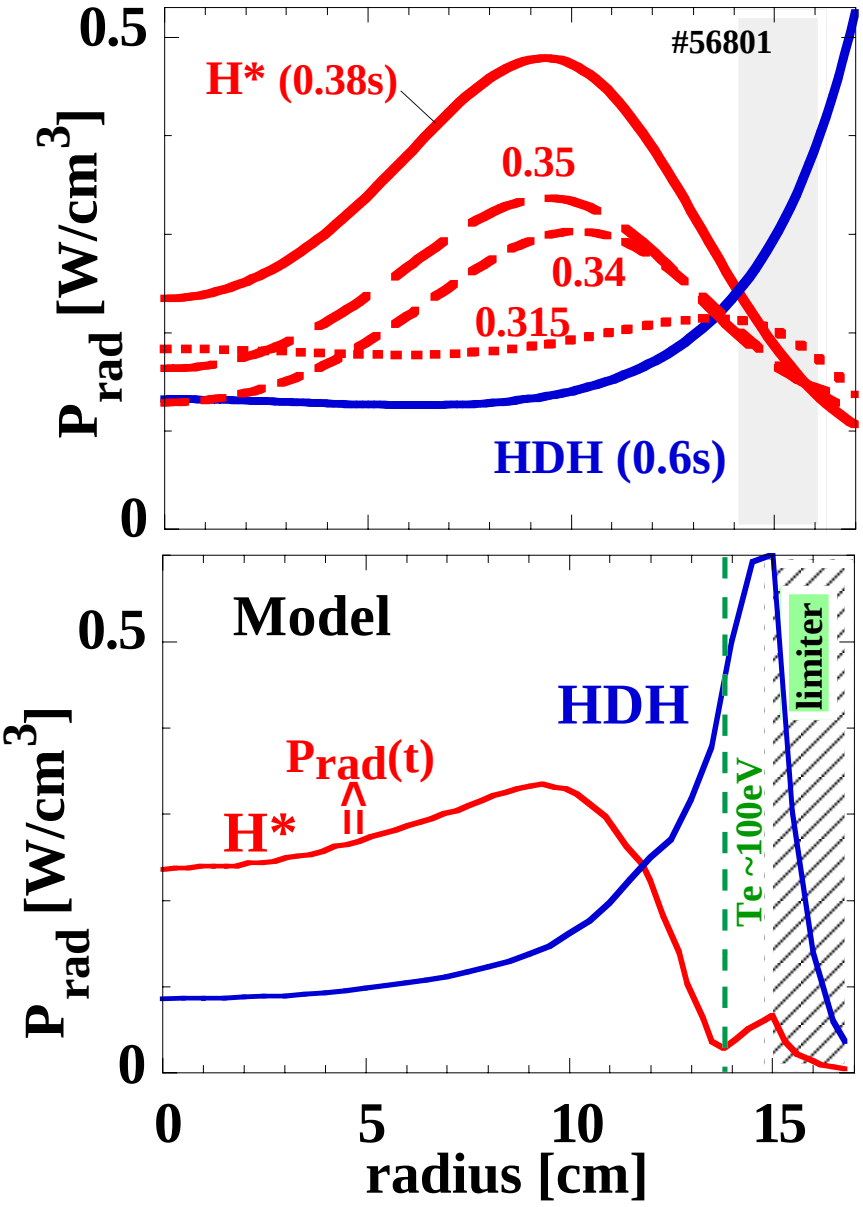


Fig. 8: Experimental (top) and modeled (bottom) $P_{rad}$ profiles. The experimental profiles are derived from a bolometer array and taken from the H*- (red) and HDH-phases (blue) of the discharge of Figs. 5-6. The approximate region of the separatrix position is indicated; uncertainties arise due to the nature of the deconvolution process. The model calculation using the SITAR code is meant to reproduce qualitative features of the experiment, not exact details. Here the same $n_e$- and $T_e$-profiles are taken for both H* and HDH simulations (#55542 of Fig. 4), with the difference being that an enhanced impurity diffusion coefficient is present in the edge gradient region for HDH and not for H*. Impurities (carbon, iron) are released from the limiter and penetrate into the core plasma. In this limiter situation, the point where $T_e$~100eV is marked, and may be taken as roughly equivalent to the separatrix position for a divertor configuration. Note that the H* situation leads to a continuous increase in $P_{rad}$ with time over the time scale of the experiment. Here only one time slice is shown.